Lab on a Chip

Devices and applications at the micro- and nanoscale

Accepted Manuscript

This article can be cited before page numbers have been issued, to do this please use: J. Doon-Ralls, S. Mayone, X. Y. Rima, D. Shantaram, K. T. Nguyen, A. Singh, B. J. Needleman, S. Noria, S. Brethauer, K. A. Perry, D. Wood, A. D. Jalilvand, W. A. Hsueh and E. Reátegui, *Lab Chip*, 2026, DOI: 10.1039/D5LC01156F.

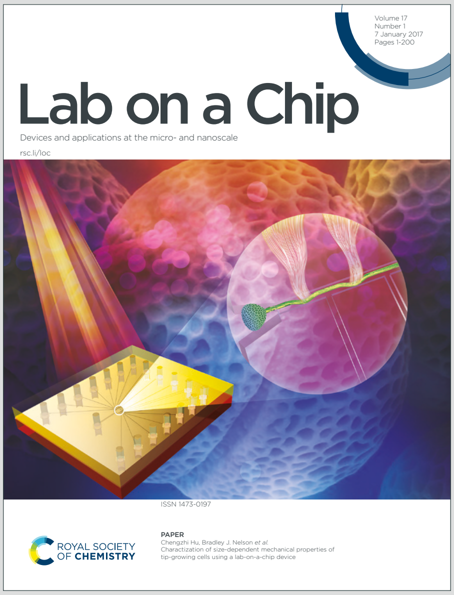
Volume 17
Number 1
7 January 2017
Pages 1-200

Lab on a Chip

Devices and applications at the micro- and nanoscale

rsc.li/loc

ISSN 1473-0197

ROYAL SOCIETY OF CHEMISTRY

PAPER
Chengzhi Hu, Bradley J. Nelson *et al.*
Charactization of size-dependent mechanical properties of tip-growing cells using a lab-on-a-chip device

ROYAL SOCIETY OF CHEMISTRY

rsc.li/loc

View Article Online
DOI: 10.1039/D5LC01156F

View Article Online
DOI: 10.1039/D5LC01156F

Tunable Self-Assembling Cellular Microarray for Single-Neutrophil Vital and Suicidal Extracellular Traps

Jacob Doon-Ralls[1,2], Sophia Mayone[1], Xilal Y. Rima[1,3], Dharti Shantaram[3], Kim Truc Nguyen[1], Ajeet Singh[1], Bradley J. Needleman[4], Sabrena Noria[4], Stacy Brethauer[4], Kyle A. Perry[4], David Wood[1], Anahita D. Jalilvand[4], Willa Hsueh[3] and Eduardo Reátegui[1,5]

[1]Department of Chemical and Biomolecular Engineering, The Ohio State University, 151 W. Woodruff Ave., Columbus, 43210, Ohio, USA.

[2]Clinical and Translational Science Institute, The Ohio State University Wexner Medical Center, 376 W. 10th Ave. Room 260, Columbus, 43210, Ohio, USA.

[3]Diabetes and Metabolism Research Center, Division of Endocrinology, Diabetes and Metabolism, Department of Internal Medicine, The Ohio State University Wexner Medical Center, 473 W. 12th Ave., Columbus, 43210, Ohio, USA.

[4]Department of Surgery, The Ohio State University Wexner Medical Center, 395 W. 12th Ave., Columbus, 43210, Ohio, USA.

[5]Comprehensive Cancer Center, The Ohio State University, 460 W. 10th Ave., Columbus, 43210, Ohio, USA.

Corresponding Author: reategui.8@osu.edu

View Article Online
DOI: 10.1039/D5LC01156F

Abstract

Neutrophils, the innate immune system's first line of defense, function in pathogen removal through diverse cellular responses. One critical response is neutrophil extracellular trap (NET) formation, which, despite its importance in inflammation, remains poorly understood and lacks high-resolution tools to effectively study its multiple forms: vital and suicidal. To begin addressing this gap, we introduce a tunable micropatterned platform that enables single-cell analysis of NETosis with spatial precision. Using photopatterned bacterial extracellular vesicles (bEVs) on a functionalized surface, we achieved controlled alignment of human peripheral blood neutrophils and demonstrated that engineered patterns control key NETosis outcomes. While PMA stimulation induced uniform suicidal NETosis. This approach supports additional applications, enabling tunable neutrophil patterning and live-cell imaging for intracellular investigation. Additionally, there is flexibility for different extracellular vesicle and nanoparticle patterning and pre-stimulation studies. Here, we present a novel system to quantify and manipulate NETosis pathways at the single-cell level, opening new avenues to explore immune heterogeneity and develop targeted therapies.

View Article Online
DOI: 10.1039/D5LC01156F

Introduction

The innate immune system's first line of defense is comprised of leukocytes called neutrophils[1]. Neutrophils are polymorphonuclear granulocytes that make up 40 – 70% of white blood cells[2] which function in pathogen and cellular debris removal through various cellular responses, and play a role in inducing the immune signaling cascade[3]. These responses include the complex multicellular and intricately controlled process of neutrophil swarming and crowding[4], as well as phagocytosis[5], reactive oxygen species (ROS) generation[6], and neutrophil extracellular trap (NET) formation[7]. All these processes can activate other immune cells and are critical for neutrophil function and for maintaining immune system homeostasis.

NETosis, a neutrophil function which is not a multicellular response, is a neutrophil-specific type of cell death where traps are released into the extracellular space containing histones, chromatin, and/or mitochondrial DNA[8, 9]. The specific type of NETosis determines what is released. Suicidal NETosis involves the complete decondensation of the nucleus through peptidyl arginine deiminase 4 (PAD4) activation, spewing histones, chromatin, neutrophil elastase (NE) and myeloperoxidase (MPO) around itself and at its target resulting in cell death[10]. In contrast, vital NETosis has two independent mechanisms: one where PAD4 is activated and chromatin is decondensed and packaged into vesicles along with proteins used in pathogen elimination (e.g., MPO and NE)[11], and another where mitochondrial DNA[12] is packaged into vesicles and released. (**Fig. 1A**) These neutrophils remain vital, maintaining the ability to phagocytose and respond to chemotaxis[13].

Many engineered techniques have been developed to study the diverse functions of neutrophils. These include patterning clusters of Bioparticles™ to initiate neutrophil swarming with microscopic analysis[14], designing PDMS chambers to enclose one to four neutrophils and capture released NETs[15], and creating devices to capture NETs themselves to study their effects on different bacterium[16]. However, none of these techniques consistently achieve single-cell resolution, and they only study the effects of suicidal NETosis. Additionally, the engineering of matrix-bound extracellular vesicles (EVs) has produced a lot of interest recently in vesicle-mediated cellular control[17, 18], especially as previously reported with light-induced extracellular vesicle and particle adsorption (LEVA), which utilized bacterial EVs (bEVs) to induce neutrophil swarming against different micropatterns of bEVs[19]. These detailed bEV micropatterns are currently a limitation of lithography techniques to make traditional microfluidic devices via replica molding with PDMS[20, 21]. LEVA is much more versatile thanks to a digital micromirror device, which enables high spatial resolution with rapid temporal throughput.

Here, we present a tunable, self-assembling single-neutrophil NETosis device. Where LEVA has been expanded to produce high-resolution grids of bEVs at the size of a single cell to further investigate the effects of matrix-bound EVs on immune cell function. Here, neutrophils are consistently patterned down to single-cell resolution along this grid of bEVs, allowing the study of both suicidal and vital NETosis within the same device, depending on the desired outcome. The bEVs are patterned along a uniform 100x100 array of 16π μm^2 area shapes, onto which neutrophils can self-assemble and undergo the desired NETosis.

View Article Online
DOI: 10.1039/D5LC01156F

Results

bEV Characterization, Isolation and Photopatterning

To produce the stimuli needed for neutrophil patterning and vital NETosis induction, the Escherichia coli (*E. coli)* pET/eGFP-streptII-his6 plasmid (**Fig. 2A**) was transformed into competent BLR(DE3) cells, which allowed them to express enhanced green fluorescent protein (eGFP)[22], ensuring the encapsulation of this desired protein into the bEVs[19]. BEVs are known to be mostly produced during cell division[23]; therefore, induction was targeted at the late log phase for optimal production. After the cells and large debris were pelleted, the bEVs in the broth needed to be purified from excess proteins; therefore, tangential flow filtration (TFF) was utilized (**Fig. 2B**). In this process, the bEVs were contained in the retentate while the unwanted proteins and small molecules were eluted out through continuous diafiltration with phosphate buffer solution (PBS). This method has been validated by our group to produce extracellular particles of increased purity[24]. To quantify bEV concentration and size distribution, tunable resistive pulse sensing was utilized, which shows the homogenous size distribution peak with a right-side tail due to sterile filtering **(Fig. 2C**). A transmission electron microscopy (TEM) image of purified bEVs validates this size distribution and allows for the identification of the lipid bilayer and the purity of the sample (**Fig. 2D**). For bEV photopatterning, we used LEVA[19]. Briefly, a clean, plasma-treated glass coverslip was coated with an electrostatically active polymer, poly-L-lysine (PLL). The PLL was covered with a non-biofouling polymer, methoxy-poly(ethylene glycol)-succinimidyl valerate (mPEG-SVA), and after the addition of a photoactivator, was cleaved upon UV exposure, leaving the revealed PLL to electrostatically adhere the bEVs. Neutrophils were added atop of them, where they began to recognize the bEVs and self-patterned onto the photo-etched, bEV filled, regions, a schematic is outlined in **Fig. 2E**.

Neutrophil Self-Patterning

Four different pattern shapes were engineered for testing the stimulation of NETosis. Each pattern had unique characteristics: a circle, a half-circle with a pointed end (called ‘ice cream cone’), a capital “I”, and lastly a 4-point star (**Fig. 3A**). The circular pattern was designed to maintain uniformity of the cell. The ice cream cone pattern was designed as an asymmetric pattern. Furthermore, the capital “I” pattern was designed to test the neutrophils' coverage, and the “4-point star” pattern was designed to test the stretch of the neutrophil in a symmetric way. F-actin staining validates the conformity to these shapes (**Fig. 3D** and **Sup. Fig. 1**). All these patterns were designed to maintain a uniform area 16π μm^2, the area of the 8μm diameter circle, so that the same number of bEVs can adhere to each photoetched region. At a resolution down to 2 μm, bEVs had electrostatically adhered to the photopatterned regions (**Fig. 3B**). When neutrophils were added they took the shape of the desired patterns, indicating that the design activates the neutrophils (**Fig. 3C**). This effect was observed from a wide field of view of a 23x23 array of bEV patterns, showcasing the expandability of this platform (**Fig. 3D**). The combination video of all neutrophil differential shape patterning and NETosis along with a control of no patterned bEVs highlights the unique properties of each pattern (**Sup. Vid. 1**). Depending on the desired cell density per pattern, a variable number of cells were added per unit of patterned area. At the lowest concentration, nearly 90% of the filled patterns contained a single cell, which decreased to 60%

View Article Online
DOI: 10.1039/D5LC01156F

at the highest concentration (**Fig. 3E**). This enabled users to tune the number of cells per pattern, whether they were studying single- or multi-cell interactions, with representative images of 2,000 and 3,000 cells / mm^2 (**Sup. Fig. 2A and B**).

Neutrophil Nucleus Decondensation

Through fluorescence microscopy and single-cell patterning, we investigated nuclear changes in neutrophils. Neutrophils aligned onto the bEV pattern were stained with live-cell stains preemptively and visualized through both phase-contrast (**Fig. 4A**) and fluorescence imaging (**Fig. 4B**). Here, Hoechst 33342 was utilized to visualize real-time nucleus dynamics, a critical aspect of NETosis, with arrows identifying some NETosis, where the nucleus was initially seen as multi-lobed throughout the cells and underwent decondensation as NETosis progressed. A zoomed-in region on one specific cell (**Fig. 4C**) aided in the identification of nuclear decondensation. The nuclear roundness (**Eq. 1**), which is the inverse of aspect ratio, was initially irregular, and as time progressed, and neutrophils underwent NETosis, it became more rounded (**Fig. 4D**). Similarly, nuclear circularity (**Eq. 2**) was initially irregular, and as time progressed and the nuclear envelope decondensed during NETosis, the circularity metric approached one (**Fig. 4E**). Circularity highlights the perimeter smoothness and roundness highlights elongation symmetry; both together give a more complete picture of nuclear morphology. Furthermore, in some large vesicles produced during vital NETosis (**Sup. Fig. 3A**), parts of the nucleus were observed inside vesicles, and with a dead cell stain present, no free DNA was stained, as during vital NETosis the membrane remains intact (**Sup. Fig. 3B**).

$$Equation\ 1. \qquad Roundness = \frac{4 * Area}{\pi * Major\ Axis\ Length^2}$$

$$Equation\ 2. \qquad Circularity = \frac{4\pi * Area}{Perimeter^2}$$

Vital and Suicidal NETosis Induction

Neutrophils that were self-patterned via the bEVs underwent vital NETosis, as seen through the rapid vesiculation and protrusions produced from the neutrophil's membrane (**Fig. 5A**). There was substantial heterogeneity in vital NET production, where no two cells undergoing vital NETosis were identical (**Sup. Fig. 3C** and **Sup. Vid. 2**). Due to staining of the nucleus and cytoplasm, these vesicles and protrusions were visualized and identified (**Fig. 5B**). The ice cream cone patterned bEVs induced NETosis in up to 70% of the neutrophils, which was different from other patterns tested (**Fig. 5E**). The distribution of NETosis points can be seen with the mean number of cells at each timepoint for each shape conditions (**Sup. Fig. 4**). When 4nM of phorbol 12-myristate 13-acetate (PMA) was added to the already patterned neutrophils to induce suicidal NETosis, the cells appeared white under phase contrast, but transitioned to a darker color, indicating membrane disruption and suicidal NETosis (**Fig. 5C** and **Sup. Fig. 5**). To validate suicidal NETosis, the nucleus and dead cell stain, along with a fluorescently conjugated MPO antibody were colocalized (**Fig. 5D** and **Sup. Fig. 5**). Throughout the duration of the assay, 100% of the cells underwent suicidal NETosis consistently along the same timeline (**Fig. 5F**). PMA at 4nM was validated for the induction of suicidal NETosis, where it began with limited dead cells and MPO signal with intact nuclei, but after 4 hours, there was substantially more MPO signal

View Article Online
DOI: 10.1039/D5LC01156F

which colocalized with extracellular DNA and the original membrane-permeable DNA stain, as seen in the zoomed-in region (**Sup. Fig. 5**). To further validate suicidal NETosis, a conjugated anti-H3 Histone (citrulline R2 + R8 + R17) antibody was utilized to observe the presence of citrullinated H3 histones post 4nM PMA stimulation (**Sup. Fig. 6**). Furthermore, to verify vital NETosis, a PAD4 inhibitor (PAD4i, GSK484) was utilized at 10μm[25, 26] where it was seen that there was no nuclear decondensation (**Sup. Fig. 7A**), followed by a reduction in nuclear roundedness and circularity (**Sup. Fig. 7B**). Additionally, less than 5% of cells underwent vital NETosis during PAD4i (**Sup. Fig. 7C**). Moreover, to verify the vital NETosis was not apoptosis, a commercial apoptosis indicator (YO-PRO-1, a non-membrane permeable DNA stain) was utilized. This stain was not present during vital NETosis protrusion formation and only became fluorescent post-vital NETosis (**Sup. Fig. 8**). Additionally, to verify the vital NETosis was not necroptosis, a conjugated anti-MLKL (phosphor S358) antibody was utilized to observe the lack of signal during vital NETosis (**Sup. Fig. 9**).

Differential NETosis Through Multiple Stimuli

An advantage of LEVA is that it allows the user to pattern biological and non-biological materials, including other mammalian EVs (from individual cells or donor plasma) and gold nanoparticles (AuNPs) (**Fig. 6A**). Therefore, we investigated whether these alternative EVs/NPs could stimulate NET production. Different patterned NP subtypes induced varying levels of neutrophil activation (**Fig. 6D**), which led to differential amounts of both vital (**Fig. 6E**) and suicidal NETosis (**Fig. 6F**). Where representative images showcase the neutrophils undergoing NETosis (**Fig. 6C**). The NETosis data can be combined to view total NETosis (**Fig. 6G**) and due to the uniqueness of this platform to differentiate NETosis types, new inferences can be made regarding the differences in vital, suicidal or total NETosis. The area under the curve (AUC) was calculated via the trapezoid rule, and statistical significance was observed between data sets (**Fig. 6H**). There was a significant difference between patterned obese and lean AdEVs for vital NETosis AUC, but no significant difference for suicidal or total NETosis AUC. Conversely, obese plasma EPs produced a significant difference against all other conditions for suicidal NETosis AUC, but when total NETosis AUC was compared, there was no significance between obese plasma EPs and bEVs. An additional avenue of investigation was to perturb the neutrophils with different stimuli before addition to the patterned bEV array. Here, we stimulated neutrophils with lean or obese AdEVs before the bEV array (**Fig. 6B**). Due to obese AdEVs stimulation, an increase in vital NETosis was observed compared to the bEVs alone, while lean AdEVs followed the bEVs-alone trend (**Fig. 6I**). The AUC was compared across the conditions and identified that the obese AdEVs caused a significant increase in vital NETosis compared to the lean AdEVs and bEVs alone (**Fig. 6J**). This begins to showcase the endless possibilities enabled through this platform.

Discussion

The reported results identified the self-patterning of neutrophils down to single-cell resolution on an array of a functionalized surface that contained precisely patterned bEVs. This allows for specific spatial control of neutrophils. Once the neutrophils had self-aligned onto the bEV array, two types of NETosis were quantified, depending on the desired outcome. An additional means of controllability within this assay was the precise patterning of a desired number of neutrophils, through adjusting cell concentration. Vital NETosis has been implicated in a multitude of

View Article Online
DOI: 10.1039/D5LC01156F

diseases[27], but the commercially available method for studying NETosis[27] only allows for the study of suicidal NETs released from bulk neutrophils. While there has been limited knowledge of vital NETosis, its implications in diseases remain unknown[28]. Additionally, technologies are advancing towards the study of single cells, such as with gene or protein expression[29], fluorescent-activated flow sorting[30], and laser scanning cytometry[31], due to understanding the heterogeneity of cell populations[32], especially within neutrophils[33]. Therefore, it is critical to include that in the design specifications of new *in vitro* assays. There has been much research on neutrophil swarms of different sizes recently[14], and this was the first method which consistently produced neutrophil crowds of one, two or three cells, which specifically allows the user to study cell-to-cell relations directly as they cooperatively interact with pathogenic particles. Therefore, this assay is the first of its kind to have single-cell resolution with the ability to tune the number of cells per pattern while also allowing the investigator to control the NETosis of interest.

Furthermore, combining our assay with live-cell microscopy enabled intracellular investigation, identifying real-time, live-cell, cytochemistry. We demonstrated proof of concept through staining and study of nuclear decondensation, which is critical to both vital and suicidal NETosis; however, many different live cell stains can also be utilized. For example, mitochondrial stains could investigate the importance of mitochondrial fusion or fission during NETosis, which has been of interested during neutrophil swarming[14]. pH-sensitive dyes can be utilized to understand a variety of cellular functions, where early and late endosomes and lysosomes become progressively more acidic. The free pH-sensitive dye can identify endocytosis and pinocytosis, and conjugated dyes or ligands can enable the study of receptor or ligand mediated endocytosis and antibody internalization. Moreover, cytoskeleton dyes can enable studies of cytoskeleton dynamics and how the vesicles produced during vital NETosis are organized, packaged and expelled.

Additionally, an interesting aspect of this platform was that it enabled investigating cell decision-making, which has been of interest in recent publications[34], both in the context of neutrophil migration[35] and the neutrophil's path to either phagocytose or NETose[36]. However, these publications lacked the resolution and spatial control achievable with this platform and either focused on migration or suicidal NETosis. Therefore, this assay offers a unique capability to investigate fundamental neutrophil decisions regarding which NETosis pathway they will execute. As we observed, not all cells underwent vital NETosis, which again offers a unique ability to study this heterogeneous process, suggesting that intrinsic variability could control it. This opens avenues for investigating molecular checkpoints which bias neutrophils towards distinct pathways, with implications for understanding immune regulation in infection, autoimmunity and sepsis. Whereas other neutrophil responses are irreversible, such as swarming[4], the reversible nature of vital NETosis provides a unique opportunity to study versatile strategies that neutrophils employ under stress.

“Moreover, there are relevant applications of this technology in translational science and clinical outcomes. This technology can study the complexity of NETosis from patient blood samples. Such as how NETosis has been implicated in immunothrombosis, sepsis and autoimmune diseases. NET-induced immunothrombosis results in more robust thrombi with less penetrability and reduced sensitivity to lysis[37]. Additionally, H3 histone levels were found to inversely relate with ICU recovery, antithrombin and platelet levels[38]. Furthermore, NET-related immunothrombosis,

View Article Online
DOI: 10.1039/D5LC01156F

histones and cell-free DNA have been associated in mortality and morbidity of sepsis[39, 40]. For autoimmune diseases inefficient NETs clearance has been identified in lupus nephritis patients[41] and in small-vessel vasculitis neutrophil-associated antibodies can cause NET formation[42]. Further reinforcing the idea that this technology can be applied to clinical samples and result in new information and studies of complex NETosis related diseases."

Our study focused on *E. coli* bEVs, which acted as a standard baseline for NETosis induction and were useful for causing neutrophil alignment, but this also means that there are many open avenues to study different bacterial EVs. Specific bacteria are known to be implicated in many diseases, ranging from respiratory[43], skin and soft tissue[44], sexually transmitted[45] and rare / emerging infections[46]. In many of these cases how the first line of defense, i.e. neutrophils, acts against these bacteria is unknown. Even more unknown is the implication of these different bacterial EVs and how they impact neutrophil function[47], while what is known is that bacterial EVs can be immunomodulatory[48] and affect many bacterial functions[49]. Additionally, biofilms produce the most bEVs[50]; therefore, this technology allows for a new route to investigate how biofilms, such as dental plaque[51], impact neutrophil function through bEV production. This new technology opens an emerging field of understanding the importance of bEVs and their influence on immune cell function.

In this study, we take an important step enabling high-resolution studies of NETosis. Adapted from a novel LEVA method, the rapid and scalable micropatterning of bEVs is easy to use and robust enough for translational studies while requiring only a small sample size of cells (<30,000). We show that we can provide spatial control of neutrophils through pattern design, spacing and surface engineering to produce single-neutrophil patterns. In LEVA, chemotactic accumulation of neutrophils occurred due to the micropattern size. More importantly, during this process, we lost track of cells once they joined the swarm, a key difference of the present application, in which we can follow the changes of neutrophils as they undergo NETosis. This assay is the first of its kind to allow simultaneous study of different types of NETosis while employing the advanced imaging techniques required to capture these events. This platform offers opportunities to explore microenvironmental cues, pathogen-derived vesicles or therapeutic agents that influence neutrophil behavior. Further studies could leverage this approach to investigate signaling pathways that govern NETosis decisions and immune heterogeneity. Given the ability to engineer the surface and patterns to desired specifications, this method offers a unique means to investigate neutrophil NETosis at a single-cell resolution *in vitro* for fundamental research and translational applications.

Materials and Methods

Empty and eGFP Bacterial Extracellular Vesicle Growth

The 1341_pET_Empty vector or pET/EGFP-strep-his plasmids were used to produce the empty or eGFP BEVs, respectively. These plasmids were obtained from the Wood Lab strain collection (Ohio State University, OH, USA). The plasmids were miniprepped according to the manufacturer's protocol (Qiagen) and transformed into competent *E. coli* BLR (DE3) cells. A 10 mL primary culture of Luria Broth media with 100 µg/mL ampicillin was inoculated with a single colony and grown for 18 hours at 225 revolutions per minute (rpm) and 37°C. The 10 mL primary

View Article Online
DOI: 10.1039/D5LC01156F

culture was then added to 1 L of Terrific Broth media with 100 µg/mL ampicillin in a 2.5 L Thompson Ultra Yield™ flask (Oceanside, CA, USA). This culture grew at 37°C and 275 rpm to an optical density of 600 nm of 3 ± 0.5. Once this threshold was reached, the culture was induced with isopropyl-β-D-1-thiogalactopyranoside at a final concentration of 0.5 mM. The culture was then incubated at 275 rpm at 16°C for 16 hours. The culture was centrifuged at 8,000 x g to pellet the whole cells and large vesicles, leaving the bEVs in the supernatant. This supernatant was stored at –80°C until further purification.

For further purification, the conditioned media containing the bEVs was thawed at 4°C overnight and sterile vacuum-filtered through a 0.2 µm filter (Corning, Cat#430769). The bEV media was further enriched and purified using tangential flow filtration with a molecular weight cut-off (MWCO) of 500 kDa using polysulfone hollow fiber filter cartridges (Repligen, Cat#D02-D500-05-N) with seven dia-cycles. The enriched media was then further concentrated using a 50 kDa spin filter (Amicon, REF#UFC805024) at 3,000 x g until the desired volume was achieved. The resulting bEVs were aliquoted and stored at –80°C until characterization and use.

Bacterial Extracellular Vesicle Characterization

All bEVs were characterized using tunable resistive pulse sensing (TRPS) and transmission electron microscopy (TEM). TRPS was performed with the qNano Gold (Izon) using a 200 nm nanopore (NP200), calibrated with a standard 200 nm polystyrene particle (CPC200) at a voltage of 0.28 V, stretch of 46.5 mm and pressure of 5 mbar. A total of 500 particles were counted to generate concentration and size distribution profiles. For negative-staining TEM preparation, the TEM grid was exposed to oxygen plasma for 1 minute. The grid was then incubated with a concentrated bEVs solution for 1 minute to allow adsorption of the bEVs to the surface. The adsorbate was removed using filter paper, and the adsorbent was sequentially washed twice with droplets of water for injection (WFI). The grid was then placed into negative stain (UranyLess EM Stain, Electron Microscopy Sciences) for approximately 22 seconds, with excess stain removed using filter paper. The TEM grid was left to dry overnight. TEM imaging was performed using a Tecnai TF-20 microscope (FEI Company, Hillsboro, OR) operating at 200 kV. eGFP bEVs were further characterized via fluorescent imaging using total internal reflective fluorescence microscopy (TIRFM) on a Nikon Eclipse TI-2 (Nikon, Tokyo, Japan) equipped with a 100x oil immersion lens.

Adipocyte Extracellular Vesicle Isolation

Fresh adipose tissue was collected from lean and obese patients undergoing elective surgery. All human adipose studies were approved by The Ohio State University Institutional Review Board (IRB #2014H0471). Fresh adipose tissue (AT) (5–20 g) was processed within 30 minutes of procurement. The tissue was then minced and digested with collagenase buffer (Gey's balanced salt solution, Sigma G9779; 1 M HEPES, Gibco 15630-080; 10% BSA, Fisher Bioreagents BP1605-100; 5 mM adenosine, Thermo Scientific A10781.09; and collagenase II, Worthington Biochemical LS004176) for 45 minutes at 37°C. Digested AT was filtered through 500 µm and 300 µm filters, respectively, followed by centrifugation at 1100 rpm for 10 minutes at 4°C. The top layer of adipocytes was gently separated from the media, leaving the stromal vascular fraction (SVF) as the bottom pellet. Mature adipocytes were then cultured in media containing high-

View Article Online
DOI: 10.1039/D5LC01156F

glucose DMEM, 10 µM insulin, antibiotics (penicillin/streptomycin), and EV-free fetal bovine serum (FBS; Gibco Cat# A2720801), ensuring that collected EVs originated solely from the mature adipocytes. The adipocytes were cultured for 18-24 hours at 37°C. Cell culture media (CCM) was then collected and subjected to gradient centrifugation to remove adipocytes, leaving EVs produced by the adipocytes in the supernatant. The CCM was processed via TFF in the same manner described above for the bEVs.

Neutrophil Isolation

All experiments were performed in accordance with the Guidelines of the Office of Research at The Ohio State University, and the Experiments were approved by the ethics committee and the biomedical science committee with Institutional Review Board (IRB) number 2018H0268 at The Ohio State University. Informed consents were obtained from human participants of this study. Human peripheral blood was collected in K2-Ethylenediaminetetraacetic acid (EDTA), purple top, tubes (BD Vacutainer, Fisher Scientific). At a 1:20 ratio the fresh blood was added to an RBC lysis buffer solution of 10mM sodium bicarbonate, 150mM ammonium chloride and 0.1mM EDTA at a pH of 7.4 for 5 minutes. The remaining solution is centrifuged at 350 x g for 5 minutes to isolate the white blood cells, while the supernatant is discarded. The neutrophils were isolated using immuno-magnetic negative selection with the EasySep^{TM} Human Neutrophil Isolation Kit (STEMCELL Technologies, Vancouver, Canada) according to the manufacturers protocol. The neutrophils were stained in serum free Iscove's Modified Dulbecco's Medium (IMDM, ThermoFisher) and 1% penicillin-streptomycin (PS, Gibco, Thermofisher) with 1.5µM of CellTracker Green (ThermoFisher) for 30 minutes while during the last 15 minutes 20 µg/mL Hoechst 33342 (Thermofisher) was added. Once the desired time has elapsed, 1.5x the cell volume of PBS was added to the cells and staining solution, and the neutrophils were spun down at 190 x g for 5 minutes to be resuspended in their working media. The final neutrophil suspension was at 6×10^5 cells / mL in IMDM with 20% fetal bovine serum (FBS, Gibco, Thermofisher) and 1% PS. 1% PS was included in the final suspension to reduce the potential for microbial contamination that could introduce unintended neutrophil activation. For AdEV stimulated neutrophils, the desired number of cells were aliquoted and stimulated with 10,000 AdEVs per cell for 1 hour prior to addition to the bEV pattern.

Light-Induced Patterning

Adapted from previously reported Light-induced Extracellular Vesicle Adsorption technique[19]. Initially, glass coverslips (Fisherbrand Cat#12541027) were cycled between ethanol and deionized (DI) water for 3 sonication cycles to ensure cleanliness. The surface of the coverslip was then activated via oxygen plasma for 1 minute and a silicone well (Grace Biolabs, GBL103280) was placed atop the glass. Into the wells, a 0.01% (w/v) poly-L-lysine (PLL) was incubated on the surface for 1 hour. Following 3 washings of 0.1M caustic HEPES buffer the surface was incubated with 100 mg/mL methoxy-poly(ethylene glycol)-succinimidyl valerate (mPEG-SVA) diluted in 0.1M HEPES buffer for 1 hour. The surface was rinsed in DI water and dried under nitrogen flow before a benzophenone based photoactivator, 4-benzoylbenzyl-trimethylammonium chloride (PLPP, AveoleLabs), diluted in 96% Ethanol was placed onto the surface through evaporative deposition. The coverslips were photoetched utilizing a digital micro-mirror optical module (PRIMO, AveoleLabs) mounted on an automated inverted microscope

View Article Online
DOI: 10.1039/D5LC01156F

(Nikon Eclipse, TI), with a resolution down to 2μm. The UV dose was 30mJ/mm^2. The patterns were designed with the microscope camera resolution of 0.29μm / pixel for area calculations. The remaining PLPP was washed away with DI water, and the surface was dried under nitrogen flow. The surface was rehydrated with phosphate buffer solution (PBS) for 5 minutes followed by E11 bEVs being added to adsorb to the photoetched regions for 5 additional minutes, followed by 10 washes of PBS. The surface was coated with FBS for 5 minutes to aid in neutrophil adhesion. Please find the schematic of this workflow in **Fig. 2E**.

Neutrophil Patterning

50μL of cell solution was added to a well and the cells were allowed to settle on the patterned bEVs surface to align themselves for 1-hour at 37°C. For 4nM PMA addition, the supernatant was gently removed and replaced with media spiked with 4nM PMA containing 1μm SYTOX Orange^{TM} to identify extracellular DNA, FITC-conjugated anti-MPO (1:100 dilution, Abcam Cat# ab11729) and/or AlexaFluor^{TM} 488-conjugated anti-H3 Histone (citrulline R2 + R8 + R17, 1:100 dilution, Abcam Cat# ab281584), to allow for the real time quantification of suicidal NETosis. 4nM PMA was chosen as 4-times the concentration utilized in a commercial NETosis assay kit (Caymen Chemical, Item No. 601010). This is done 3 times to ensure the media contacting the cells was at the desired concentration of PMA (4nM), stain and/or antibodies, then sealed with a 12mm round coverslip. For no PMA addition, the supernatant was gently removed and replaced with media spiked with YO-PRO-1 (1:2000 dilution), AlexaFluor^{TM} 488-conjugated anti-MLKL (phosphor S358, 1:100 dilution, Abcam Cat# ab187091), 10μM GSK484 (Abcam Cat# ab223598) and/or 1μm SYTOX Orange^{TM}, then the wells were sealed with a 12mm round coverslip. What was included in either of these additions depended on what was of interest to the specific experiment. Anti-MLKL and Anti-H3 Histone were AlexaFluor^{TM} 488-congugagted via a ReadyLabel^{TM} Antibody Labeling Kit (ThermoFisher, Cat# R10712) following the manufacturers protocol. F-actin was stained post 4% paraformaldehyde fixation and Triton TE buffer permeabilization using ActinRed^{TM} 555 ReadyProbes^{TM} regent (ThermoFisher, Cat# R37112) and imaged via total internal reflection fluorescence microscopy (Nikon Ti2).

Live Cell Imaging and NETosis Quantification

Once the neutrophils have been patterned, the device was then added to an inverted epifluorescent microscope (Nikon Ti2) equipped with stage-top incubator (Ozark) set at 37°C, 21% O_2 and 5% CO_2, and imaged every 5 minutes for 8 hours. The data files were processed via FIJI. Vital NETosis was quantified via the cell counter plugin within FIJI, where the protrusions produced were identified and counted. The threshold for vital NETosis was these protruding vesicles being expelled ≥ ¼ cell diameter, persisting for ≥ 5 minutes (2 frames), ≥ 5 vesicles and without extracellular DNA staining (measured through SYTOX^{TM} Orange). Suicidal NETosis was quantified also via the cell counter plugin within FIJI, identifying where there was colocalization with Hoechst 33342, SYTOX^{TM} Orange and the FITC-conjugated anti-MPO.

Statistical Analyses

All statistical analyses were performed via JMP Pro 18. All experiments were performed as biological triplicates with technical replicates, supplied in the figure captions. Pairwise

View Article Online
DOI: 10.1039/D5LC01156F

comparisons were performed via two-tailed *t*-tests. Analysis of variance was performed for multiple samples, followed by Tukey's HSD for multiple comparisons.

Author Contributions

J.D.R. and E.R. designed the study. J.D.R. conducted the experiments, performed data analysis, prepared the figures and wrote the initial manuscript. K.T.N. performed TEM preparation and imaging. A.D.J., B.J.N., S.N., S.B. and K.A.P. obtained clinical samples. X.Y.R. and D.S. processed clinical samples. S.M. and D.W. provided bacteria supernatant containing bEVs. J.D.R., S.M., X.Y.R., D.S., K.T.N., A.S., A.D.J., W.A.H. and E.R. contributed to interpretation of results, discussed experiments, contributed to the article and edited the manuscript. W.A.H. acquired additional funding, provided mentorship and oversight to the study.

Conflicts of Interest

There are no conflicts to declare.

Acknowledgements

We thank our healthy donors who donated blood enabling the healthy neutrophil studies. This work was supported by funding from the William G. Lowrie Department of Chemical and Biomolecular Engineering, the Comprehensive Cancer Center at The Ohio State University, the National Institute of Health grants: UH3TR002884 (E.R.), U18TR003807 (E.R.), T32TR004543 (J.D.R.), KL2TR001068 (W.A.H.), HL135622 (W.A.H.) and T32HL149637 (X.Y.R.), American Diabetes Association grant 1-16-ICTS-049 (W.A.H.), American Heart Association grant 24PRE1243747 (D.S.) and Burroughs Wellcome Fund Postdoctoral Enrichment Program 1285320 (X.Y.R.)

Data Availability Statement

The data supporting the findings of this study are available from the corresponding author upon reasonable request.

View Article Online
DOI: 10.1039/D5LC01156F

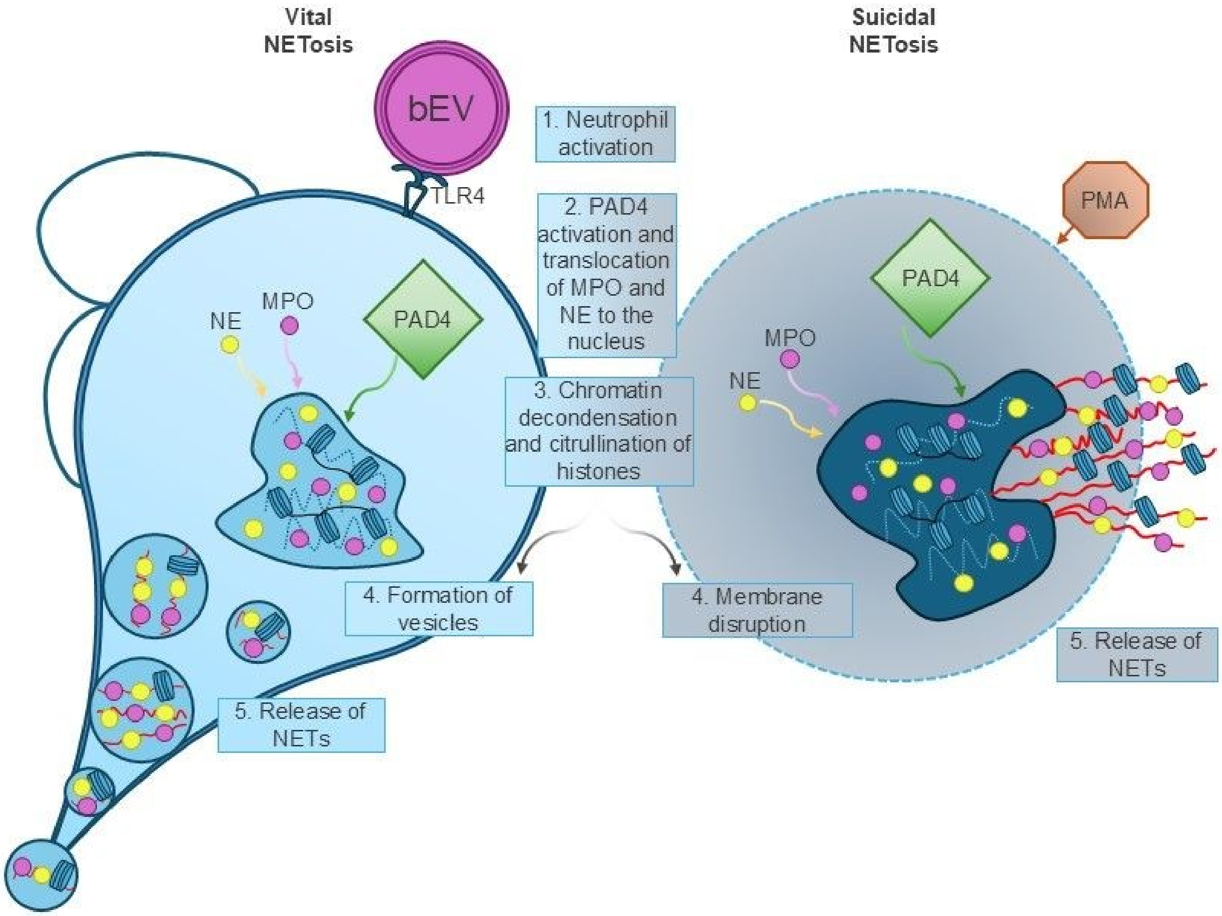

Fig. 1. NETosis. Schematic classifying vital (left) vs. suicidal (right) NETosis.

View Article Online
DOI: 10.1039/D5LC01156F

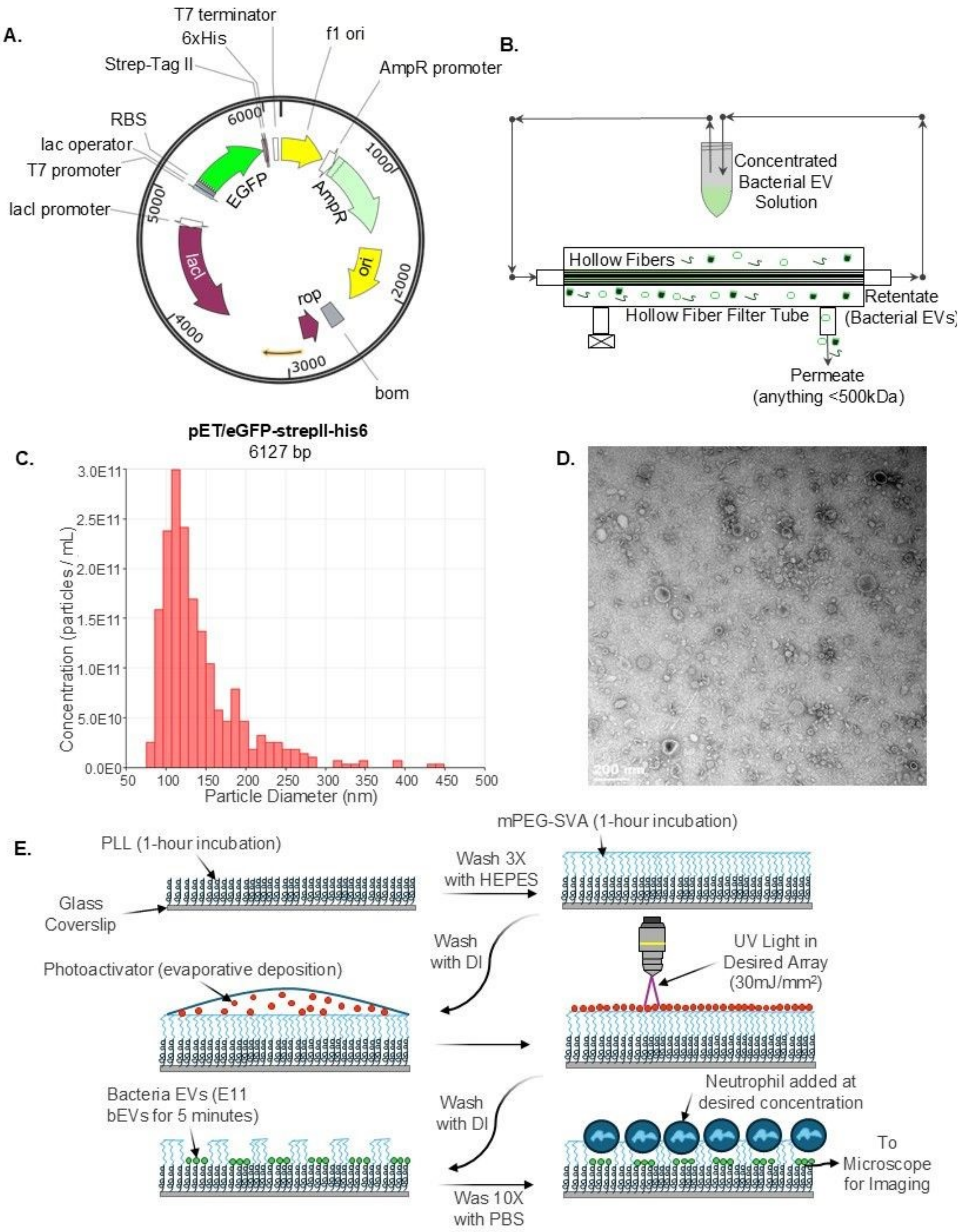

Fig. 2. BEV Production, Isolation, Characterization and Patterning Schematic. (A) Plasmid used to cause eGFP expression in *E. coli*. (B) TFF schematic to identify bEV purification technique. (C) bEV size distribution measured through TRPS (n = 500 bEVs). (D) TEM image of bEVs (scale bar = 200nm). (E) Schematic identifying the surface chemistries necessary for neutrophil patterning, through the coating of PLL, mPEG-SVA and photoactivator, into UV exposure to selectively allow bEVs to pattern, followed by the addition of neutrophils.

View Article Online
DOI: 10.1039/D5LC01156F

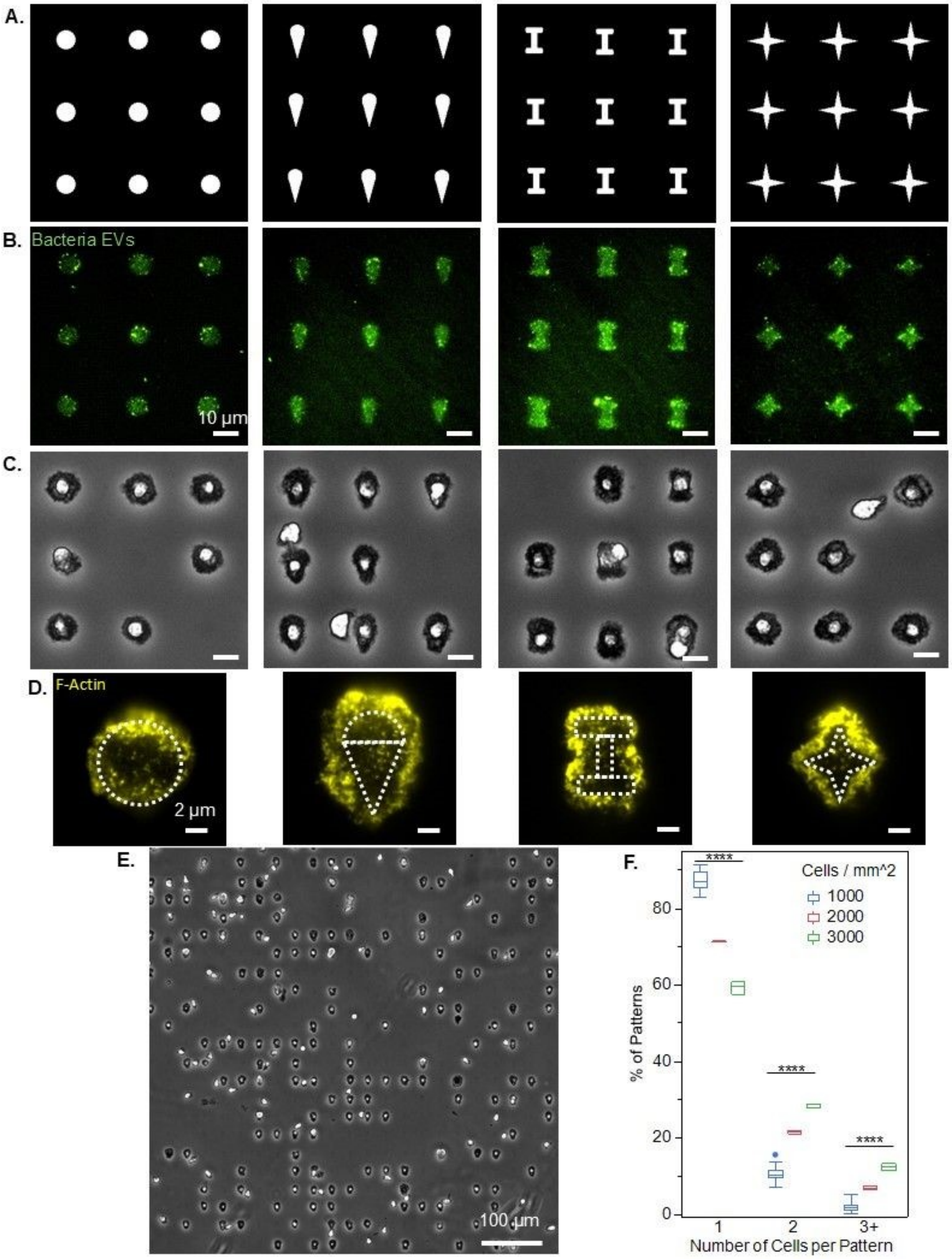

Fig. 3. Single Neutrophil Patterning on Different Shapes. (A) Gray-scale photomask for selective cleavage. (B) BEV pattern in the UV exposed regions. (C) Neutrophil patterning and taking the desired shape (B/C scale bars = 10μm). (D) Neutrophil F-Actin staining while on each patterned shape (Scale Bar = 2μm) (E) Wide-field image of neutrophils on the patterned regions (scale bar = 100μm). (F) Graph identifying the number of cells per pattern depending on different seeding densities. (**** indicates p < 0.0001 across the 3 densities, Tukey's HSD, N = 3 biological replicates of separate healthy donors and n = 600 cells from 3 independent fields of view).

View Article Online
DOI: 10.1039/D5LC01156F

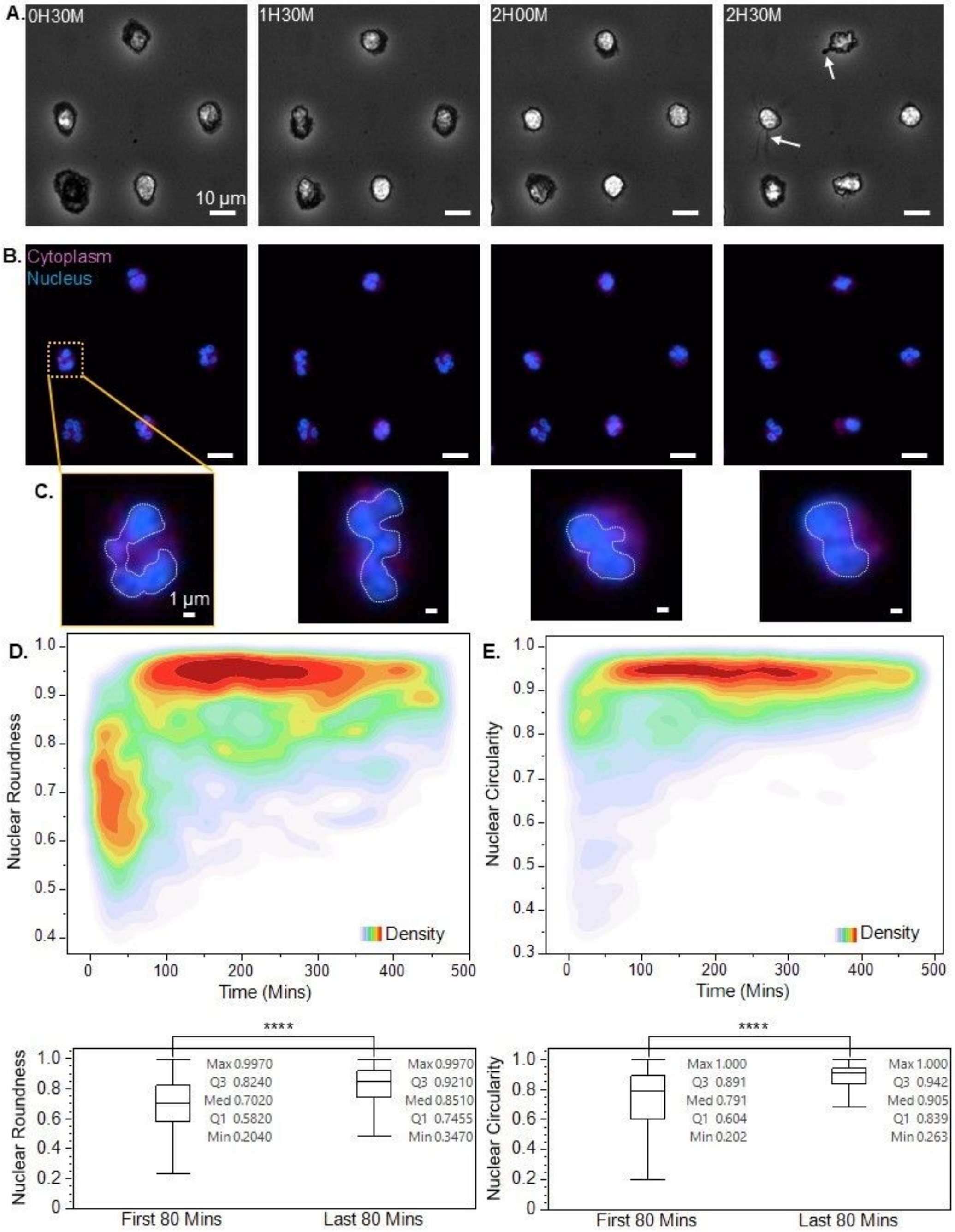

Fig. 4. Looking at Nuclear Decondensation Inside the Neutrophil. (A) Phase-contrast images at different time-points with arrows identifying protrusions produced during vital NETosis. (B) Fluorescent images at the same time-points identifying nuclear decondensation. (purple = cytoplasm and blue = nucleus, A/B scale bars = 10μm) (C) Zoomed in image of one nucleus with a dashed line to aid in the identification of the nuclear envelope. (purple = cytoplasm and blue = nucleus, scale bar = 1μm) (D and E) Neutrophil nuclear roundness (D) and circularity (E) throughout the duration of the experiment (n=250 cells, bar graphs for the first and last 80 minutes of the experiment, **** denotes p < 0.0001 Student's T-Test).

View Article Online
DOI: 10.1039/D5LC01156F

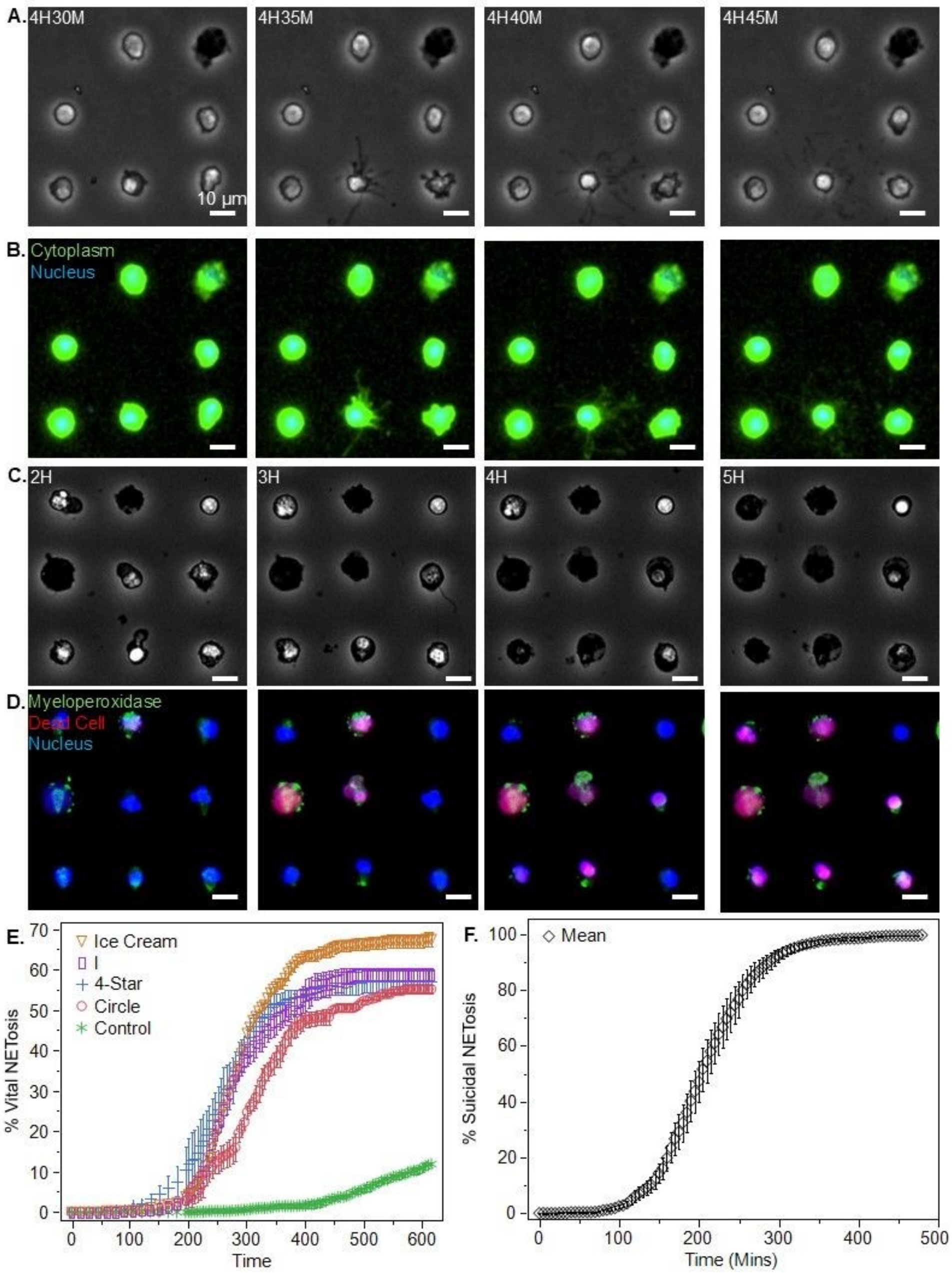

Fig. 5. Vital and Suicidal NETosis Induction. (A) Phase contrast images 5 minutes apart displaying the vesiculation and ejection of internal components during vital NETosis. (B) Fluorescent images during the same time frames as (A) identifying the cytoplasmic contents of the vesicles (Blue = nucleus and Green = cytoplasm). (C) Phase contrast images 1 hour apart displaying the membrane disruption and ejection of internal components during suicidal NETosis. (D) Fluorescent images during the same time frames as (C) identifying the free DNA and MPO present during suicidal NETosis (green = MPO, blue = membrane permeable DNA stain, red = non-membrane permeable DNA stain and A/B/C/D scale bars = 10μm). (E) Differential vital NETosis induction based on the shape pattern. (F) Suicidal NETosis time dependence graph (error bars in E and F represent standard error, N = 3 biological replicates of separate healthy donors and n = 600 cells from 3 independent fields of view).

View Article Online
DOI: 10.1039/D5LC01156F

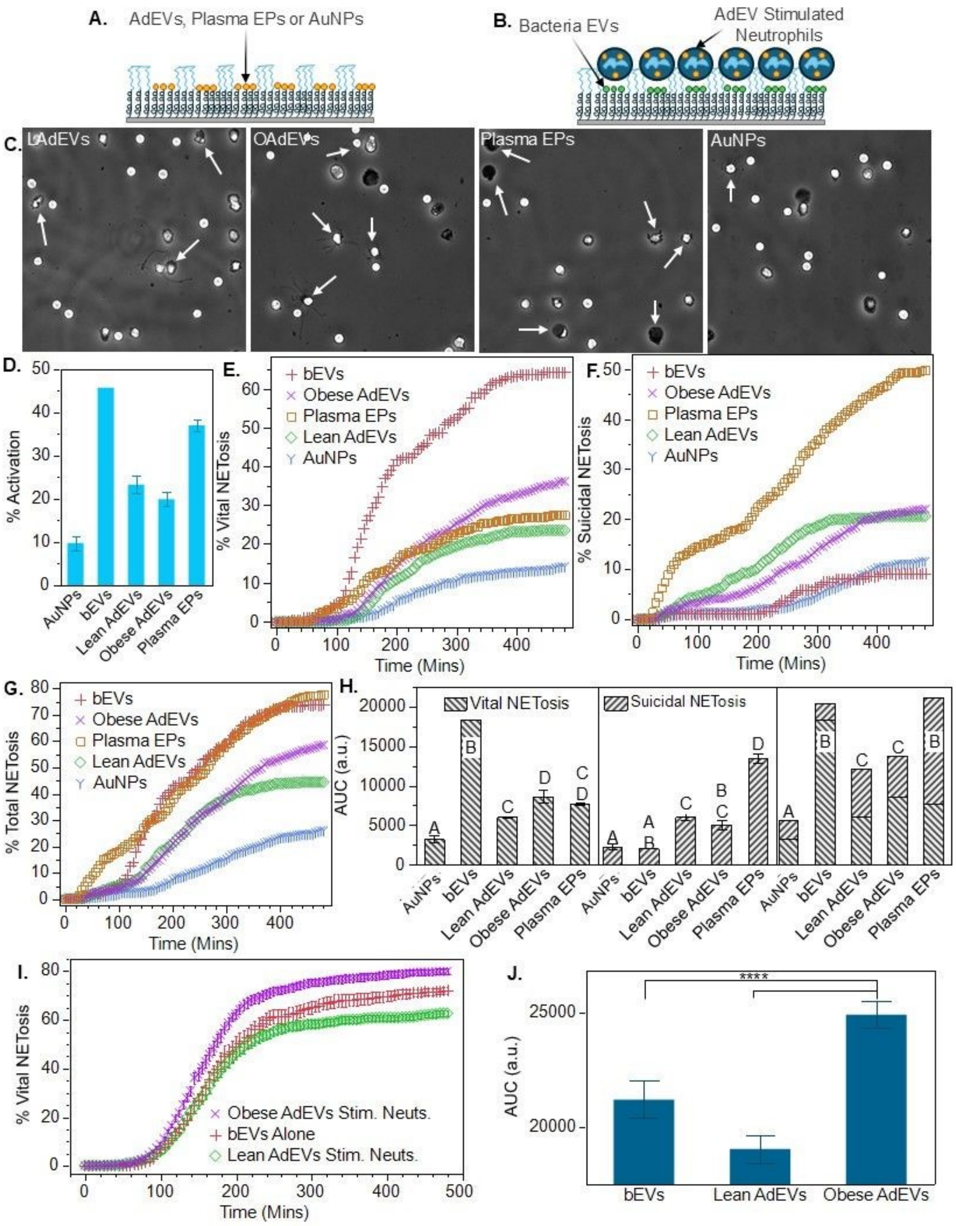

Fig. 6. Differential NETosis Through Multiple Stimuli. (A) Schematic of patterned Adipocyte extracellular vesicles (AdEVs), plasma extracellular particles (EPs) or gold nanoparticles (AuNPs). (B) Schematic of AdEV-stimulated neutrophils on top of the bEV pattern. (C) Representative images of the patterned AdEVs, Plasma EPs and AuNPs (scale bar = 25μm). (D) Percent activation of neutrophils on the different patterned materials. (E) Vital, (F) suicidal and (G) total NETosis induction from the different patterned materials. (H) Area under the curve (AUC) for each of the different patterned materials (left to right) for vital, suicidal and total NETosis induction (connecting letters report to identify significance α = 0.05, Tukey's HSD). (I) Vital NETosis from neutrophils stimulated with lean or obese AdEVs and bEVs alone. (J) AUC for the AdEV stimulated neutrophil graph (**** denotes $p<0.05$, Tukey's HSD, N = 3 separate lean and obese AdEV samples tested with 1 healthy neutrophil donor, with n = 600 cells counted from 3 independent fields of view, error bars in D-J represent Standard Error).

View Article Online
DOI: 10.1039/D5LC01156F

References.

1. J. Parkin and B. Cohen, Lancet, 2001, 357, 1777-1789.
2. C. Kantari, M. Pederzoli-Ribeil and V. Witko-Sarsat, Contrib Microbiol, 2008, 15, 118-146.
3. W. M. Nauseef and N. Borregaard, Nat Immunol, 2014, 15, 602-611.
4. T. Lämmermann, P. V. Afonso, B. R. Angermann, J. M. Wang, W. Kastenmüller, C. A. Parent and R. N. Germain, Nature, 2013, 498, 371-375.
5. O. Soehnlein and L. Lindbom, Nat Rev Immunol, 2010, 10, 427-439.
6. N. Borregaard, K. Theilgaard-Mönch, J. B. Cowland, M. Ståhle and O. E. Sørensen, J Leukoc Biol, 2005, 77, 439-443.
7. T. A. Fuchs, U. Abed, C. Goosmann, R. Hurwitz, I. Schulze, V. Wahn, Y. Weinrauch, V. Brinkmann and A. Zychlinsky, J Cell Biol, 2007, 176, 231-241.
8. E. Pérez-Figueroa, P. Álvarez-Carrasco, E. Ortega and C. Maldonado-Bernal, Front Immunol, 2021, 12, 631821.
9. F. V. S. Castanheira and P. Kubes, Blood, 2019, 133, 2178-2185.
10. A. Hidalgo, P. Libby, O. Soehnlein, I. V. Aramburu, V. Papayannopoulos and C. Silvestre-Roig, Cardiovasc Res, 2022, 118, 2737-2753.
11. V. Papayannopoulos, Nat Rev Immunol, 2018, 18, 134-147.
12. C. Lood, L. P. Blanco, M. M. Purmalek, C. Carmona-Rivera, S. S. De Ravin, C. K. Smith, H. L. Malech, J. A. Ledbetter, K. B. Elkon and M. J. Kaplan, Nat Med, 2016, 22, 146-153.
13. B. G. Yipp and P. Kubes, Blood, 2013, 122, 2784-2794.
14. K. M. Glaser, J. Doon-Ralls, N. Walters, X. Y. Rima, A. S. Rambold, E. Réategui and T. Lämmermann, iScience, 2024, 27, 108656.
15. U. S. Datla, B. Vundurthy, J. S. Hook, N. Menon, H. Razmi Bagtash, T. Shihabeddin, D. W. Schmidtke, J. G. Moreland, M. Z. Radic and C. N. Jones, Lab Chip, 2024, 24, 615-628.
16. M. Sakuma, A. Viens, A. Hopke, D. J. Floyd, M. Ghebremichael, M. K. Mansour and D. Irimia, J Leukoc Biol, 2025.
17. G. Rackov, N. Garcia-Romero, S. Esteban-Rubio, J. Carrión-Navarro, C. Belda-Iniesta and A. Ayuso-Sacido, Front Physiol, 2018, 9, 651.
18. K. Rilla, A. M. Mustonen, U. T. Arasu, K. Härkönen, J. Matilainen and P. Nieminen, Matrix Biol, 2019, 75-76, 201-219.
19. C. L. Hisey, X. Y. Rima, J. Doon-Ralls, C. K. Nagaraj, S. Mayone, K. T. Nguyen, S. Wiggins, K. D. P. Dorayappan, X. Huang, Hade, M.D., K. Selvendiran, J. N. Higginbotham, O. Tutanov, J. L. Franklin, Coffey, R.J., D. Wood, C. Hu, D. Patel, S. M. Magaña, A. F. Palmer, D. Hansford and E. Reátegui, 2025, **22**, 2609-2621.
20. O. C. a. R. L. a. G. M. Vera Faustino and Susana, Journal of Biomechanics, 2016, 49, 2280-2292.
21. V. C. Pinto, P. J. Sousa, V. F. Cardoso and G. Minas, Micromachines, 2014, 5, 738-755.
22. D. A. Zacharias, J. D. Violin, A. C. Newton and R. Y. Tsien, Science, 2002, 296, 913-916.
23. M. G. Sartorio, E. J. Pardue, M. F. Feldman and M. F. Haurat, Annu Rev Microbiol, 2021, 75, 609-630.

View Article Online
DOI: 10.1039/D5LC01156F

24. J. Zhang, L. T. H. Nguyen, R. Hickey, N. Walters, X. Wang, K. J. Kwak, L. J. Lee, A. F. Palmer and E. Reátegui, Sci Rep, 2021, 11, 8034.
25. X. Xia, Z. Zhang, C. Zhu, B. Ni, S. Wang, S. Yang, F. Yu, E. Zhao, Q. Li and G. Zhao, Nat Commun, 2022, 13, 1017.
26. H. D. Lewis, J. Liddle, J. E. Coote, S. J. Atkinson, M. D. Barker, B. D. Bax, K. L. Bicker, R. P. Bingham, M. Campbell, Y. H. Chen, C. W. Chung, P. D. Craggs, R. P. Davis, D. Eberhard, G. Joberty, K. E. Lind, K. Locke, C. Maller, K. Martinod, C. Patten, O. Polyakova, C. E. Rise, M. Rüdiger, R. J. Sheppard, D. J. Slade, P. Thomas, J. Thorpe, G. Yao, G. Drewes, D. D. Wagner, P. R. Thompson, R. K. Prinjha and D. M. Wilson, Nat Chem Biol, 2015, 11, 189-191.
27. N. V. Vorobjeva and B. V. Chernyak, Biochemistry (Mosc), 2020, 85, 1178-1190.
28. S. S. Burgener and K. Schroder, Cold Spring Harb Perspect Biol, 2020, 12.
29. J. Kehr, Curr Opin Plant Biol, 2003, 6, 617-621.
30. J. P. Nolan and L. A. Sklar, Nat Biotechnol, 1998, 16, 633-638.
31. M. M. Harnett, Nat Rev Immunol, 2007, 7, 897-904.
32. J. L. Spudich and D. E. Koshland, Nature, 1976, 262, 467-471.
33. H. Raskov, A. Orhan, S. Gaggar and I. Gögenur, Oncogenesis, 2022, 11, 22.
34. A. P. Coulibaly, Immunol Rev, 2022, 311, 177-186.
35. B. P. Boribong, M. J. Lenzi, L. Li and C. N. Jones, Front Immunol, 2019, 10, 359.
36. S. Boeltz, P. Amini, H. J. Anders, F. Andrade, R. Bilyy, S. Chatfield, I. Cichon, D. M. Clancy, J. Desai, T. Dumych, N. Dwivedi, R. A. Gordon, J. Hahn, A. Hidalgo, M. H. Hoffmann, M. J. Kaplan, J. S. Knight, E. Kolaczkowska, P. Kubes, M. Leppkes, A. A. Manfredi, S. J. Martin, C. Maueröder, N. Maugeri, I. Mitroulis, L. E. Munoz, D. Nakazawa, I. Neeli, V. Nizet, E. Pieterse, M. Z. Radic, C. Reinwald, K. Ritis, P. Rovere-Querini, M. Santocki, C. Schauer, G. Schett, M. J. Shlomchik, H. U. Simon, P. Skendros, D. Stojkov, P. Vandenabeele, T. V. Berghe, J. van der Vlag, L. Vitkov, M. von Köckritz-Blickwede, S. Yousefi, A. Zarbock and M. Herrmann, Cell Death Differ, 2019, 26, 395-408.
37. I. Varjú, C. Longstaff, L. Szabó, Á. Farkas, V. J. Varga-Szabó, A. Tanka-Salamon, R. Machovich and K. Kolev, Thromb Haemost, 2015, 113, 1289-1298.
38. K. C. Wildhagen, M. A. Wiewel, M. J. Schultz, J. Horn, R. Schrijver, C. P. Reutelingsperger, T. van der Poll and G. A. Nicolaes, Thromb Res, 2015, 136, 542-547.
39. S. R. Clark, A. C. Ma, S. A. Tavener, B. McDonald, Z. Goodarzi, M. M. Kelly, K. D. Patel, S. Chakrabarti, E. McAvoy, G. D. Sinclair, E. M. Keys, E. Allen-Vercoe, R. Devinney, C. J. Doig, F. H. Green and P. Kubes, Nat Med, 2007, 13, 463-469.
40. A. C. Ma and P. Kubes, J Thromb Haemost, 2008, 6, 415-420.
41. A. Hakkim, B. G. Fürnrohr, K. Amann, B. Laube, U. A. Abed, V. Brinkmann, M. Herrmann, R. E. Voll and A. Zychlinsky, Proc Natl Acad Sci U S A, 2010, 107, 9813-9818.
42. K. Kessenbrock, M. Krumbholz, U. Schönermarck, W. Back, W. L. Gross, Z. Werb, H. J. Gröne, V. Brinkmann and D. E. Jenne, Nat Med, 2009, 15, 623-625.
43. I. S. Gomes-Filho, J. S. Passos and S. Seixas da Cruz, J Oral Microbiol, 2010, 2.
44. V. Ki and C. Rotstein, Can J Infect Dis Med Microbiol, 2008, 19, 173-184.
45. C. B. Whitlow, Clin Colon Rectal Surg, 2004, 17, 209-214.
46. M. Vouga and G. Greub, Clin Microbiol Infect, 2016, 22, 12-21.

View Article Online
DOI: 10.1039/D5LC01156F

47. J. J. Kim, E. Reátegui, A. Hopke, F. Jalali, M. Roushan, P. S. Doyle and D. Irimia, Lab Chip, 2018, 18, 1514-1520.
48. A. Srivastava, S. Rathore, A. Munshi and R. Ramesh, AAPS J, 2021, 23, 30.
49. G. Magaña, C. Harvey, C. C. Taggart and A. M. Rodgers, Antibiotics (Basel), 2023, 13.
50. W. Wang, W. Chanda and M. Zhong, FEMS Microbiol Lett, 2015, 362, fnv117.
51. P. D. Marsh and D. J. Bradshaw, Journal of industrial microbiology and biotechnology, 1995, 15, 169-175.

View Article Online
DOI: 10.1039/D5LC01156F

Data Availability Statement

The data supporting the findings of this study are available from the corresponding author upon reasonable request.